Active Site of Epoxide Hydrolases Revisited: A Noncanonical Residue in Potato StEH1 Promotes both Formation and Breakdown of the Alkylenzyme Intermediate†

Ann Thomaeus,‡ Jens Carlsson,§ Johan Åqvist,§ and Mikael Widersten*,‡

Department of Biochemistry and Organic Chemistry, Box 576, Uppsala University, BMC, SE-751 23 Uppsala, Sweden, and Department of Cell and Molecular Biology, Box 596, Uppsala University, BMC, SE-751 24 Uppsala, Sweden

Received October 2, 2006; Revised Manuscript Received December 22, 2006

ABSTRACT: The carboxylate of Glu[35] in the active site of potato epoxide hydrolase StEH1 interacts with the catalytic water molecule and is the first link in a chain of hydrogen bonds connecting the active site with bulk solvent. To probe its importance to catalysis, the carboxylate was replaced with an amide through an E35Q mutation. Comparing enzyme activities using the two *trans*-stilbene oxide (TSO) enantiomers as substrates revealed the reaction with *R,R*-TSO to be the one more severely affected by the E35Q mutation, as judged by determined kinetic parameters describing the pre-steady states or the steady states of the catalyzed reactions. The hydrolysis of *S,S*-TSO afforded by the E35Q mutant was comparable with that of the wild-type enzyme, with only a minor decrease in activity, or a change in pH dependencies of k_{cat}, and the rate of alkylenzyme hydrolysis, k_3. The pH dependence of E35Q-catalyzed hydrolysis of *R,R*-TSO, however, exhibited an inverted titration curve as compared to that of the wild-type enzyme, with a minimal catalytic rate at pH values where the wild-type enzyme exhibited maximum rates. To simulate the pH dependence of the E35Q mutant, a shift in the acidity of the alkylenzyme had to be invoked. The proposed decrease in the pK_a of His[300] in the E35Q mutant was supported by computer simulations of the active site electrostatics. Hence, Glu[35] participates in activation of the Asp nucleophile, presumably by facilitating channeling of protons out of the active site, and during the hydrolysis half-reaction by orienting the catalytic water for optimal hydrogen bonding, to fine-tune the acid−base characteristics of the general base His[300].

Epoxide hydrolases (EC 3.3.2.3) catalyze the hydrolysis of epoxides to yield the corresponding vicinal diols. Members of this widespread group of enzymes are found in all life's kingdoms from bacteria and fungi to plants and animals. Established physiological roles are as follows: detoxification enzymes converting endogenous as well as exogenous toxic epoxides to less harmful products and regulators of cellular signaling mediated by epoxide-containing bioactive lipids (see refs *1* and *2* for recent reviews). In plants, epoxide hydrolases are thought to participate in pathogen defense; the diols resulting from hydrolysis of epoxy-containing hydroxy fatty acids are precursors in the synthesis of cutin (*3*) and exhibit antifungal activity (*4*). Epoxide hydrolases are enzymes that are independent of cofactors and exhibit high activity and enantioselectivity, so in addition to the biological roles of these enzymes, their potential as biocatalysts in production of fine chemicals has attracted interest in recent years and shown promising results (*5, 6*). To be able to further improve on beneficial epoxide hydrolase activities, as well as enantioselectivity, more profound knowledge of the catalytic mechanism is required.

Epoxide hydrolase catalysis has traditionally been shown to consist of four discrete catalytic steps (Scheme 1): the formation of the Michaelis complex followed by nucleophilic attack by an active site Asp carboxylate to generate an alkylenzyme intermediate. The catalytic turnover is subsequently finalized by general base-assisted hydrolysis of the alkylenzyme and product release (*7*). Previous studies of the catalytic machinery of StEH1,[1] a soluble epoxide hydrolase from potato, have identified key residues involved in catalysis: Asp[105] acting as a nucleophile and the Tyr[154]/Tyr[235] pair stabilizing the oxyanion formed during enzyme alkylation through electrophilic catalysis by contributing hydrogen bonds via the phenolic hydroxyls. The hydrolytic step is dependent on the general base properties of His[300] (*8, 9*).

The recently determined X-ray crystal structure of StEH1 (*10*) has provided further detailed information regarding the active site architecture. This new information has led to the identification of additional residues presumably involved in catalysis. One such candidate is Glu[35] which in the crystal structure is hydrogen bonded to a putative hydrolytic water molecule (Figure 1). To assess the importance of Glu[35] in catalysis, mutant E35Q was generated, and its functional properties was compared with those of the wild-type enzyme. To aid in the interpretation of the experimental data, computer simulations of acid−base characteristics of the key

† This work was supported by the Ingegerd Bergh and Carl Trygger Foundations (M.W.) and by the Swedish Research Council. A.T. is a Lawski Foundation stipendiate.

* To whom correspondence should be addressed. E-mail: mikael.widersten@biorg.uu.se. Phone: +46 (0)18 471 4992. Fax: +46 (0)18 55 8431.

‡ Department of Biochemistry and Organic Chemistry.

§ Department of Cell and Molecular Biology.

[1] Abbreviations: StEH1, epoxide hydrolase 1 from *Solanum tuberosum*; TSO, *trans*-stilbene oxide.

10.1021/bi062052s CCC: $37.00
Published on Web 02/07/2007

Scheme 1: Kinetic Mechanism of StEH1-Catalyzed Hydrolysis of TSO

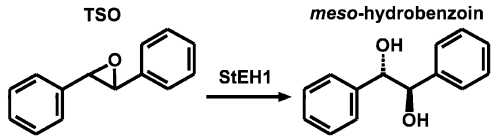

$$E + TSO \underset{}{\overset{K_S}{\rightleftharpoons}} E{\cdot}TSO \underset{k_{-2}}{\overset{k_2}{\rightleftharpoons}} E\text{-alkyl} \xrightarrow{k_3} E{\cdot}diol \overset{K_{EP}}{\rightleftharpoons} E + diol$$

catalytic residue, His[300], were performed and complemented by molecular dynamics studies.

MATERIALS AND METHODS

Structure Alignments

The SwissProt/TrEMBL database was queried with the StEH1 primary structure in BLAST searches. Hits with scores ranging from 407 to 149 ($E = 10^{-112}$ to $E = 10^{-34}$), applying the BLOSUM62 matrix, were aligned using the online facility at www.expasy.org to establish the nature of residues corresponding to StEH1 Glu[35] in related proteins.

Protein primary structures of plant and mammalian soluble epoxide hydrolases with the following entry names were extracted from SwissProt: Q41415_SOLTU, StEH1 (*11*); Q76E11_9ROSI, *Citrus jambhiri* (*12*); Q39856_SOYBN, *Glycine max* (*13*); Q8H289_ANACO, *Ananas comosus* (*14*); Q84ZZ3_EUPLA, *Euphorbia lagascae* (*15*); Q42566_ARATH, *Arabidopsis thaliana* (*16*); Q8L5G6_BRANA, *Brassica napus* (*17*); Q9S7P1_ORYSA, *Oryza sativa* (*18*); Q9ZP87_TOBAC, *Nicotiana tabacum* (*19*); HYES_PIG, *Sus scrofa* (*20*); HYES_HUMAN, *Homo sapiens* (*21*); HYES_RAT, *Rattus norvegicus* (*22*); and HYES_MOUSE, *Mus musculus* (*23*). The sequences were aligned with ClustalX 1.83 (*24*). Comparisons of conserved structure motifs were performed by superposition of the three-dimensional structures of StEH1-5H [PDB entry 2CJP (*10*)] and the epoxide hydrolase domain of human soluble epoxide hydrolase [PDB entry 1VJ5 (*25*)] using InsightII (Accelrys).

Site-Directed Mutagenesis

The E35Q mutant was constructed by inclusion of mutagenic primers (Thermo Electron Corp.) in the PCRs, using the pGTacStEH1-5H plasmid (*8*) encoding wild-type StEH1 as a template, thereby introducing a **G**AA to **C**AA codon substitution in the amplified cDNA at position 35. The E35Q cDNA fragment was subcloned between the *Mun*I and *Xho*I sites of pGTacStEH1-5H, and the plasmid construct was subsequently sequenced in full to confirm the mutation and ensure that no further alterations in the sequence had occurred.

Protein Expression and Purification

Expression plasmids encoding wild-type or mutant StEH1-5H, pGTacStEH1-5H, and pGTacStEH1-5HE35Q, respectively, were transformed into *Escherichia coli* XL1-Blue bacteria by electroporation using a Bio-Rad Gene Pulser. Protein expression and purification of the His-tagged wild-type and mutant enzymes were performed according to a previously described protocol (*8*). Homogeneities of purified protein samples were determined by SDS−PAGE with Coomassie Brilliant Blue R-250, and protein concentrations of collected fractions were determined from the absorbance at 280 nm. The used molar absorbance coefficient, calculated from the amino acid composition, was 59 030 M^{-1} cm^{-1}, and the calculated molecular mass was 37.1 kDa.

Steady State Kinetics and pH Dependencies

The wild-type and mutant epoxide hydrolase activities with both enantiomers of *trans*-stilbene oxide (TSO) were measured spectrophotometrically in 0.1 M sodium phosphate (pH 6.8) at 30 °C. Substrates were dissolved in acetonitrile and added to the reaction mixture at a final concentration of 1% (v/v) acetonitrile. The extent of hydrolysis of both enantiomers of TSO was measured as a decrease in absorbance at 229 nm ($\Delta\epsilon = -15$ mM^{-1} cm^{-1}) (*26*). For the wild-type enzyme, initial rates were recorded during the steady state in the presence of varying concentrations of *R,R*-TSO (5−40 μM) and *S,S*-TSO (0.25−20 μM). For the E35Q mutant, initial rates were recorded during the steady state in the presence of 0.39−50 μM *R,R*-TSO or *S,S*-TSO. The kinetic parameters k_{cat}, K_M, and k_{cat}/K_M were determined after fitting the Michaelis−Menten equation by nonlinear regression to the experimental data using MMFIT or RFFIT in the SIMFIT package (http://www.simfit.man.ac.uk).

Pre-Steady State Kinetics

The pre-steady state kinetic parameters were determined by studying the transient changes in the intrinsic tryptophan fluorescence of the wild type as well as mutant StEH1-5H in an SX.18MV sequential stopped-flow spectrophotometer during the reactions with the enantiomers of TSO. An excitation wavelength of 290 nm was used, and the emission was recorded after passage through a 320 nm cutoff filter. Since the two relaxation times for fluorescence decrease and recovery were on well-separated time scales, they were treated independently. The apparent rate constants were determined by fitting a single exponential with a floating end point (eq 1) to the progression curve

$$F = A \exp(-k_{obs}t) + C \quad (1)$$

where A is the amplitude of the fluorescence change, k_{obs} the observed rate constant, and C the floating end point of the progression curve. Averages of 5−12 traces were calculated and used. The pre-steady state parameters, K_S, k_2, and k_{-2}, were determined at an enzyme concentration of 2−4 μM and with varying substrate concentrations in 0.1 M sodium phosphate (pH 6.8) at 30 °C. From the observed substrate-dependent rates of the fluorescence decrease, the parameters were extracted after fitting eq 2 to the experimental data using QNFIT in the SIMFIT package.

$$k_{obs} = k_{-2} + \frac{k_2[S]}{K_S + [S]} \quad (2)$$

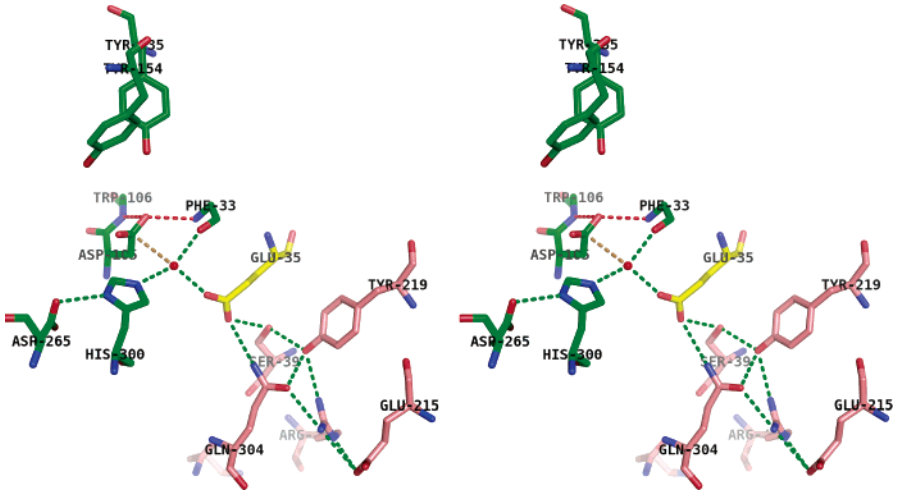

FIGURE 1: Stereoview of the location of Glu[35] in the active site of StEH1-5H. The carboxylate of Glu[35] (yellow) is within hydrogen bonding distance of the putative hydrolytic water (red sphere), the hydroxyl group of Ser[39], and the side chain amide nitrogen of Gln[304] (both latter residues colored pink). Green dashed lines indicate the hydrogen bond network (Glu[35] → Ser[39] → Tyr[219] → Arg[41] → Glu[215]) connecting the active site (center of image, Glu[35]) with bulk solvent (bottom right, Glu[215]). In the crystal structure, the catalytic water appears to be well-aligned for nucleophilic attack on the carbonyl of a putative alkylenzyme intermediate as judged by the distance and angle to the carboxylate carbon of Asp[105] (brown dashed line). The catalytic Tyr[154]/Tyr[235] pair and general base His[300] (green) as well as the backbone carbonyl oxygen hydrogen bonding to the putative hydrolytic water are indicated relative to the Asp[105] carboxylate. The location of the proposed oxyanion hole stabilizing the formed oxyanion in the hydrolytic half-reaction of catalysis (backbone amides of Phe[33] and Trp[106]) is denoted (red dashed lines) relative to the Asp[105] carboxylate. This image was created in PyMOL (*56*) by applying the atomic coordinates of 2CJP (*10*).

The parameter k_2/K_S was extracted using the same curve fitting program but using eq 3 instead.

$$k_{obs} = k_{-2} + \frac{\frac{k_2}{K_S}[S]}{1 + \frac{[S]}{K_S}} \quad (3)$$

The hydrolysis rates, k_3, were determined in single-turnover experiments by rapidly mixing equimolar amounts of enzyme (10 μM wild type or 10−20 μM E35Q mutant) and substrate (5 μM for the wild type and 8−16 μM for the E35Q mutant) and measuring the rate of fluorescence recovery after the initial burst decrease. The alkylenzyme hydrolysis was treated as a unimolecular process allowing for extraction of values of k_3 by substitution of k_{obs} with k_3 in eq 1. The reactions were carried out at 30 °C in 0.1 M sodium phosphate (pH 6.8).

pH Dependence of Kinetics

Values of k_{cat} and k_3 for wild-type and mutant enzymes with both enantiomers of TSO were determined over a pH range of 4.5−10, using the following buffers: 0.1 M sodium acetate for pH 4.5−6.0, 0.1 M sodium phosphate for pH 6.0−8.0, and 0.1 M Tris-HCl for pH 8−10. All measurements were taken at 30 °C with a maximal concentration of 2% (v/v) acetonitrile and detected as described above.

Equation 4 was fitted to the determined k_{cat} and k_3 values to extract apparent pK_a values.

$$L_H = \frac{\frac{[H^+]^2}{K_{a1}K_{a2}}L_{H_2A} + \frac{[H^+]}{K_{a2}}L_{HA^-} + L_{A^{2-}}}{1 + \frac{[H^+]}{K_{a2}} + \frac{[H^+]^2}{K_{a1}K_{a2}}} \quad (4)$$

In eq 4, L_H is the pH-dependent kinetic parameter, L_{H2A}, L_{HA-}, and L_{A2-} are the respective amounts of the different protonation states of the enzyme−substrate complexes, and K_{a1} and K_{a2} are the respective apparent acid constants.

Simulation of the pH Dependence of k_{cat}

The rate equation for invoked reaction steps contributing to observed k_{cat} values (Figure 6A) was deduced by the approach described by Waley (*27*) to yield an expression for $1/k_{cat}$. The obtained equation was inverted to result in eq 5.

$$k_{cat}^{obs} = (k_2k_3'k_3'')/[k_2k_3'(1 + K_{a3}/[H^+] + k_2k_3''(1 + [H^+]/K_{a2}) + k_3'k_3''(1 + [H^+]/K_{a1}) + k_2k_{-3}'(1 + [H^+]/K_{a2}) + k_{-2}k_{-3}'(1 + [H^+]/K_{a1}) + k_{-2}k_3''(1 + [H^+]/K_{a1})] + k_0[K_a^{1g}/(K_a^{1g} + [H^+])] \quad (5)$$

The parameters k_2 and k_{-2} are the rates of the forward and reverse reactions for alkylenzyme formation, respectively, and k_3' and k_3'' are the rates of formation and breakdown of the tetrahedral intermediate, respectively. The acid constants K_{a1}, K_{a2}, and K_{a3} describe the acidity of the enzyme−substrate complex and the alkylenzyme and tetrahedral intermediates, respectively. Parameters describing rates of breakdown of the transient tetrahedral intermediate, k_{-3}' and k_3'', were estimated to be large, due to the inherent instability of that species. Values of k_2 and k_{-2} were estimated from extrapolations of the values determined at pH 6.8 by applying an apparent pK_a of 7.5 (*9*). The added parameter k_0 is the rate of "uncatalyzed" cleavage of the alkylenzyme intermediate at the active site, treated as if it is independent of acid−base catalysis by the enzyme. The value of this rate was estimated from the asymptotes of the fitted curves to the experimentally determined pH dependence of k_{cat}. The constant K_a^{lg} is the acid constant of the conjugate acid of

the leaving group alkoxide at the active site and was set to values ranging from 8 to 12 in the simulations.

Solvent Isotope Effects of Alkylenzyme Hydrolysis

Deuterium solvent isotope effects were investigated in single-turnover condition experiments as described above, by measuring the rates of fluorescence recovery after the initial burst decrease with wild-type and E35Q mutant epoxide hydrolase hydrolyzing *R,R*-TSO. The reactions were conducted in 84.1% deuterium oxide in 0.1 M sodium phosphate with the pH varying between pH 6.2 and 10.0. The reaction buffers were produced by mixing one part of 1 M sodium phosphate buffer, in water, with nine parts of deuterium oxide (99.9%). Applying eq 6 to the displayed values compensated for the lower reading of the glass electrode in D_2O.

$$pH = pD + 0.3139\alpha + 0.0854\alpha^2 \quad (6)$$

where pD is the value from the glass electrode reading and α is the fraction of D_2O of total D_2O and H_2O.

The reactions were carried out as described above with the exception that deuterium oxide-containing buffers were used. The hydrolysis rate constants, k_3, were determined from averages of six traces using eq 1. The kinetic solvent isotope effects (k^{H_2O}/k^{D_2O}) were obtained from the ratios of the maximal rates for the wild-type enzyme, or the minimal rates for the E35Q mutant, at the respective inflection points of the fitted curves.

Computer Simulations

Docking. Docking of *R,R*-, *S,S*-TSO and the corresponding alkylenzyme intermediates was carried out with GOLD version 3.0 (*28*, *29*). For each ligand, 20 independent docking runs with default genetic algorithm search parameters were performed. The crystallographic structure of StEH1 (PDB entry 2CJP) was used as initial coordinates in all calculations. The covalent docking approach available in GOLD was used to model the alkylenzyme intermediates formed upon binding of *R,R*- and *S,S*-TSO. Since Asp[105] can attack either of the epoxide ring carbon atoms in this step, the alkylenzyme intermediate can be formed in two different ways. For each case, the carbon atom closest to Asp[105] Oδ1 in the resulting *R,R*- and *S,S*-TSO−enzyme complexes was assumed to be attacked in formation of the alkylenzyme intermediate.

Molecular Dynamics Simulations. All molecular dynamics (MD) simulations were performed with Q (*30*) using the OPLS all-atom force field (*31*). The simulations were carried out in a 20 Å sphere centered on His[300], and each system was solvated with TIP3P (*32*) water molecules. The waters on the sphere surface were subjected to radial and polarization restraints (*30*, *33*). A nonbonded cutoff of 10 Å was used, and long-range electrostatic interactions were treated with the local reaction field multipole expansion method (*34*). All atoms outside the simulation sphere were highly restrained to their initial coordinates and excluded from all nonbonded interactions. The time step was set to 1 fs, and nonbonded pair lists were updated every 25 steps. Lys[274] and all Asp, Glu, Lys, and Arg residues within 14 Å of the sphere center were set to their charged states. The protonation states for the His residues, except His[300], were set by manual inspection (uncharged for His[31], His[104], His[131], and His[153] and charged for His[269]). For His[300], both the charged and uncharged forms were simulated. Since the Nδ atom of His[300] most likely forms a strong hydrogen bond to the negatively charged carboxylate group of Asp[265], only the uncharged form of His[300] with the Nϵ position unprotonated was considered. All other ionizable residues in the system were set to their uncharged state. Simulations for wild-type and E35Q proteins were carried out for both the substrate-free and alkylenzyme intermediate states. Initial structures were obtained from the crystallographic structure (*10*) and the docking calculations described above. The E35Q mutants were created by simply replacing one of the carboxylate oxygens of Glu[35] with an NH_2 group. Each system was equilibrated by slowly heating it to 300 K while high restraints on the solute atoms to their initial coordinates were gradually released. Finally, starting from the equilibrated structure, a 250 ps fully unrestrained simulation was performed for each system.

pK_a Calculations. All calculations of pK_a values were carried out using the multiconformation continuum electrostatic (MCCE) method (*35*, *36*) in combination with Delphi (*37*). The MCCE method allows for a residue to have multiple conformational states and includes optimization of hydrogen bonds, which have been shown to increase the accuracy of calculated pK_a values significantly (*35*). Default settings, where the protein and solvent dielectric constant are set to 8 and 80, respectively, were used in all calculations. All amino acids within 4 Å of Phe[33], Glu/Gln[35], His[104], Asp[105], or His[300] were defined as "hotspots", and thereby, conformational flexibility was provided for these residues. All other atoms were fixed to their initial coordinates. The calculations were carried out for wild-type and E35Q proteins in both substrate-free and alkylenzyme intermediate forms, and all necessary input structures were extracted from the MD simulations. For each case, 10 snapshots from the MD simulations of charged and uncharged His[300] were used as starting structures in the MCCE calculations. The presented pK_a values are averages of 20 calculated values, and the errors were estimated from the standard deviations.

RESULTS

Glu[35] Is Part of a Conserved Structural Epoxide Hydrolase Motif

The crystal structure of the substrate-free StEH1-5H enzyme, at pH 7.5, points to Glu[35] as a candidate participant in the catalyzed hydrolysis of epoxides (*10*). The γ-carboxylate is within hydrogen bonding distance of a water molecule, perfectly located to act as a nucleophile in the hydrolytic half-reaction (Figure 1). The same water is also hydrogen bonded to the Nϵ atom of His[300] and the backbone carbonyl oxygen of Phe[33]. The most likely hydrogen bond pattern (Phe[33] O···HOH···Oϵ1 Glu[35]) implies that His[300] Nϵ is protonated in the substrate-free enzyme and hydrogen bonding to one of the lone pair electrons on the catalytic water. Furthermore, the water-mediated interaction between His[300] and Glu[35] forms a first link in a chain of hydrogen bonds connecting the active site with bulk solvent (Figure 1). The hydrogen bond network runs from Glu[35] → Ser[39] → Tyr[219] → Arg[41] → Glu[215], where Glu[215] situated at the protein−solvent interface participates in polar water contacts

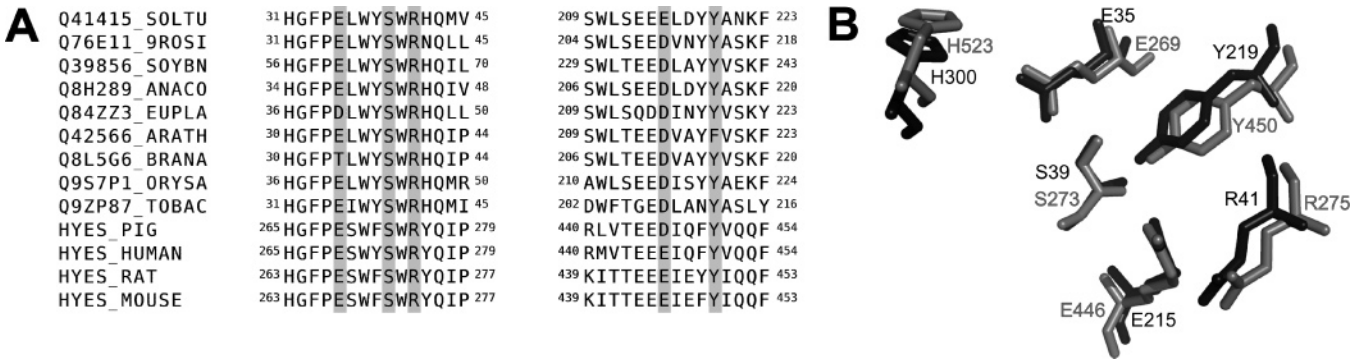

FIGURE 2: Conservation of residue functionality in a putative hydrogen bond network connecting the active site with solvent. (A) Primary structure alignment of soluble epoxide hydrolases from plants and mammals. The carboxylate groups of Glu^{35} and Glu^{215} (StEH1 numbering) are highly conserved in all sequences. Residue conservation is also observed for the functional groups corresponding to Ser^{39}, Arg^{41}, and Tyr^{219}: Q41415_SOLTU, StEH1; Q76E11_9ROSI, *C. jambhiri*; Q39856_SOYBN, *G. max*; Q8H289_ANACO, *A. comosus*; Q84ZZ3_EUPLA, *E. lagascae*; Q42566_ARATH, *Ar. thaliana*; Q8L5G6_BRANA, *B. napus*; Q9S7P1_ORYSA, *O. sativa*; Q9ZP87_TOBAC, *N. tabacum*; HYES_PIG, *S. scrofa*; HYES_HUMAN, *H. sapiens*; HYES_RAT, *R. norvegicus*; and HYES_MOUSE, *M. musculus*. (B) Superposition of the three-dimensional structures of StEH1 (black, 2CJP) and human soluble epoxide hydrolase (gray, 1VJ5) demonstrates the high degree of conservation of the interaction network also in the folded proteins.

(*10*). Comparisons of primary and tertiary structures demonstrate strong conservation of both chemical functionality and structure of the hydrogen bond network. Glu is present in 95% (89 of 94) of unique, non-potato, sequences encoding established or putative epoxide hydrolases, suggesting a function of some importance (Figure 2).

Rationale for Site-Directed Mutagenesis

To probe the role of Glu^{35} in StEH1, the carboxylate was replaced with an amide through an E35Q mutation. The orientation of the resulting amide moiety in the expressed protein is unknown but thought to place the amide NH_2 group pointing toward the hydrolytic water. The assumption is based on computer simulations of local hydrogen bond interactions in the wild-type and E35Q proteins (see below) and structural arguments; in the crystal structure of the wild-type substrate-free enzyme, the carboxylate Oϵ2 atom of Glu^{35} which interacts with the Ser^{39} hydroxyl is also hydrogen bonding to the side chain amide nitrogen of Gln^{304} (Figure 1), an interaction which is readily mimicked by the amide carbonyl oxygen in the E35Q mutant but less favorable between adjacent amide nitrogens. Additional conformers of the Gln side chain are less likely since rotation of the carboxylate/amide group is sterically restricted due to close contacts with the phenyl ring of Phe^{301}. Hence, replacing Glu^{35} with Gln is expected to alter the pattern of possible hydrogen bond donors and acceptors around the hydrolytic water, disrupting the connecting chain of hydrogen bonds from the active site His^{300} to solvent water (Figure 3). In addition, any contribution to catalysis by a general base mechanism is also abolished by the mutation.

Protein Expression and Purification

Wild-type StEH1-5H and the E35Q mutant were expressed in *E. coli* XL1-Blue and purified to homogeneity according to established procedures (*8*). Purified enzyme fractions were visualized as single protein bands on a Coomassie Brilliant Blue R-250-stained SDS−PAGE gel and were considered homogeneous. Approximately 20 mg of purified protein per liter of cultured medium was obtained. Purified proteins stored at 4 °C retained enzyme activity over the time period of analysis.

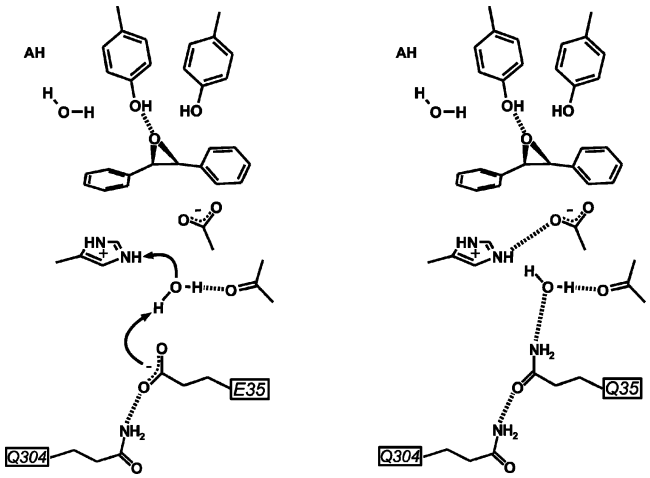

FIGURE 3: Possible effect of the E35Q mutation on hydrogen bonding in the active site. In the wild-type enzyme (left), the carboxylate oxygen of Glu^{35} is hydrogen bonded (dotted lines) to the side chain amide nitrogen of Gln^{304} well-positioned for proton abstraction of the putative hydrolytic water. Via replacement of Glu^{35} with Gln (right), an alteration of the pattern of possible hydrogen bond donors and acceptors around the hydrolytic water is anticipated, leading to a disrupted chain of hydrogen bonds from the active site His^{300} to solvent water.

Enzyme Kinetics: Hydrolysis of TSO

A full analysis of kinetic parameters for the hydrolysis of the two TSO enantiomers was conducted at pH 6.8, the established optimal pH for the wild-type enzyme (*8*). The results are listed in Table 1 and discussed below.

R,R-TSO. Hydrolysis of the *R,R* enantiomer is the reaction of the two enantiomers more severely affected by the E35Q mutation with a more than 40-fold decrease in k_{cat} compared to that of the wild-type enzyme. The effects can be traced to chemical steps of catalysis since formation of the Michaelis complex appears to be unaffected as judged by the obtained K_S value. The lowered k_{cat} is primarily caused by a 25-fold decrease in $k_3^{R,R-TSO}$. Another, unexpected effect of the mutation was a substantial, 15-fold, decrease in the rate of enzyme alkylation (k_2), resulting in a value of k_2 beginning to influence the k_{cat} rate. The slower hydrolysis rate presumably causing accumulation of alkylenzyme is further reflected in a 10-fold decrease in the value of K_M.

Table 1: Kinetic Parameters of TSO Hydrolysis Catalyzed by Wild-Type and Mutant StEH1-5H at pH 6.8

enzyme	substrate	K_S (μM)	k_2 (s^{-1})	k_{-2} (s^{-1})	k_3 (s^{-1})	k_{cat} (s^{-1})	K_M (μM)	k_{cat}/K_M (s^{-1} μM^{-1})	k_2/K_S (s^{-1} μM^{-1})
wild type	*R,R*-TSO	36 ± 22	260 ± 56	16 ± 18	24 ± 3[a]	23 ± 2[a]	10 ± 1[a]	2.4 ± 0.2[a]	7.7 ± 2.8
E35Q	*R,R*-TSO	27 ± 22	16 ± 3	6.7 ± 2	0.95 ± 0.04	0.52 ± 0.02	1.2 ± 0.1	0.48 ± 0.05	0.86 ± 0.58
wild type	*S,S*-TSO	11 ± 6[a]	18 ± 2[a]	14 ± 2[a]	3.2 ± 0.06[a]	3.8 ± 0.08	4.7 ± 0.5	0.80 ± 0.07	1.8 ± 1.4[a]
E35Q	*S,S*-TSO	≤ 5[b]	≤ 38[b]	≤ 5[b]	1.2 ± 0.06	1.2 ± 0.03	1.1 ± 0.1	1.1 ± 0.11	−

[a] Data adapted from ref *8*. [b] Poorly determined due to low signal-to-noise ratios at low *S,S*-TSO concentrations.

S,S-TSO. The reaction with the *S,S* enantiomer is virtually unaffected by the E35Q mutation, if k_{cat}/K_M values are compared. There are, however, effects which act in a compensatory manner to result in an unaltered specificity constant; both k_{cat} and K_M are 3−4-fold lower as compared to that of the wild-type enzyme. The decrease in k_{cat} is a direct reflection of a lowered alkylenzyme hydrolysis rate, k_3. A low signal-to-noise ratio at *S,S*-TSO concentrations below 20 μM precluded accurate determinations of K_S, k_2, and k_{-2}. However, the drop in alkylation rate observed in the *R,R*-TSO reaction was clearly absent with this enantiomer.

Enantiospecificity. The specificity constant of the E35Q mutant was 5-fold lower than that of the wild-type enzyme for the reaction with *R,R*-TSO. $k_{cat}/K_M^{S,S-TSO}$, however, was slightly increased due to the lower K_M displayed by the mutant. Hence, the alterations in k_{cat}/K_M caused by the mutation shifted the enantiospecificity of the wild-type enzyme from the preferred *R,R*-TSO substrate to a slight preference for the *S,S* enantiomer in the E35Q mutant.

pH Dependence of k_{cat} and k_3

The pH dependence of k_{cat} reflects the titration of ionizable groups from the Michaelis complex through the alkylenzyme intermediate leading to product. Since alkylenzyme hydrolysis is the main rate-limiting step of the overall reaction, similar titration profiles for k_{cat} and k_3 are expected and have been demonstrated previously in the StEH1-5H-catalyzed hydrolysis of *S,S*-TSO (*9*). This is also the case here, with certain deviations. The $k_{cat}^{R,R-TSO}$ of the wild-type enzyme displays a bell-shaped pH dependence with apparent pK_a values of 5.4 and 8.3, respectively (Figure 4A and Table 2). The titration of $k_3^{R,R-TSO}$ largely follows the pH dependence of k_{cat} (Figure 5A), in accordance with previously reported data for the catalyzed hydrolysis of *S,S*-TSO (*9*).

Also in the case of the E35Q mutant, titrations of k_{cat} and k_3 follow the same patterns, with distinct base and acid titrations (Figures 4 and 5). The pH dependence of *S,S*-TSO hydrolysis is similar to that of the wild-type enzyme, with a minor elevation of the apparent pK_a of the basic limb of the titration profile (Table 2). With *R,R*-TSO, however, although apparent acid constants are similar to those of the corresponding wild-type values, the pH dependence of the measured rates is inverted; the pK_a of the acidic limb resembles that of an acid titration and the more basic pK_a that of a base titration (Figure 4A). The pH profile for $k_3^{R,R-TSO}$ follows that of k_{cat}, but due to the inverted pH profiles of the E35Q mutant, the measured rates reach their minima in the same pH range in which the wild-type enzyme displays maximal rates.

To investigate possible reasons for the unexpected pH dependence displayed by $k_{cat}^{R,R-TSO}$ in the E35Q-catalyzed reaction, the k_{cat}-determining reaction steps were simulated.

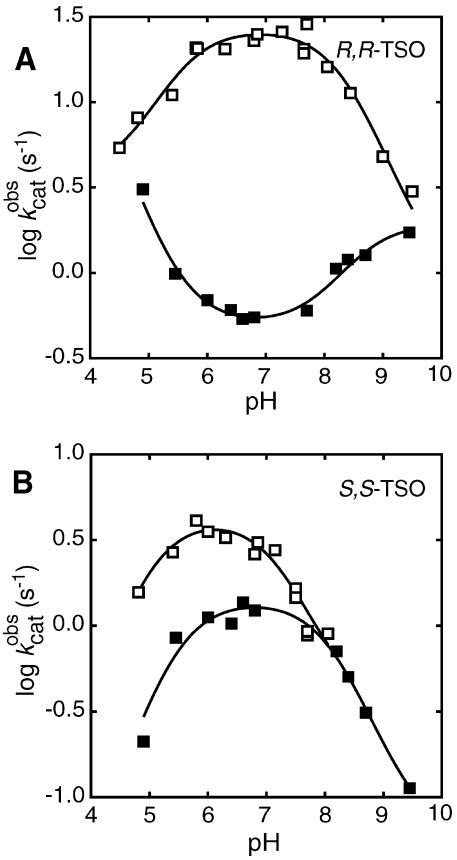

FIGURE 4: Effect of pH on the catalytic turnover, k_{cat}, for wild-type StEH1-5H-catalyzed (□) or E35Q mutant-catalyzed (■) reactions with *R,R*-TSO (A) and *S,S*-TSO (B). Lines represent the fits of eq 5, describing titration of a doubly ionizing system, to the experimental data.

The simulations are based on the assumption that the kinetic mechanism of rate-limiting steps follows the scheme shown in Figure 6A, including three acid−base equilibria as well as two distinct rates for formation and breakdown of the tetrahedral intermediate. The corresponding rate equation (eq 5) allowed for modeling of the experimentally determined pH profiles of k_{cat} (Figure 6B) entering estimated parameter values (Table 3). It became clear from the results that (a) to simulate the inverted pH profile of $k_{cat}^{R,R-TSO}$ displayed by the E35Q mutant, a substantial decrease in the rate of formation of the tetrahedral intermediate together with drastic shifts in the acidity of all enzyme−substrate/intermediate species has to be invoked (Table 3). Already, small alterations to the applied estimated acid constants given in Table 3 perturb the simulated pH dependencies of k_{cat} from the experimentally determined. The observed differences in the pH profiles of the reactions with *S,S*-TSO can be simulated by a decrease in the rate of formation of the tetrahedral intermediate and a modest increase in the acidity of the alkylenzyme intermediate. (b) To obtain simulated curves

Table 2: Experimentally Determined Apparent pK_a Values of StEH1-Catalyzed TSO Hydrolysis

	R,R-TSO				*S,S*-TSO			
	k_3		k_{cat}		k_3		k_{cat}	
enzyme	pK_{a1}	pK_{a2}	pK_{a1}	pK_{a2}	pK_{a1}	pK_{a2}	pK_{a1}	pK_{a2}
wild type (H_2O)	6.8 ± 0.2	7.8 ± 0.2	5.4 ± 0.2	8.3 ± 0.2	nd[a]	7.4 ± 0.2[b]	5.2 ± 0.5	7.4 ± 0.2
wild type (D_2O)	7.2 ± 0.5	7.9 ± 0.4	–	–	–	–	–	–
E35Q (H_2O)	7.0 ± 0.1	7.9 ± 0.3	5.5 ± 0.1	8.4 ± 0.1	6.0 ± 0.4	7.4 ± 0.1	5.3 ± 0.2	8.1 ± 0.1
E35Q (D_2O)	7.3 ± 0.2	8.4 ± 0.4	–	–	–	–	–	–

[a] Not determined. [b] Data adapted from ref *9*.

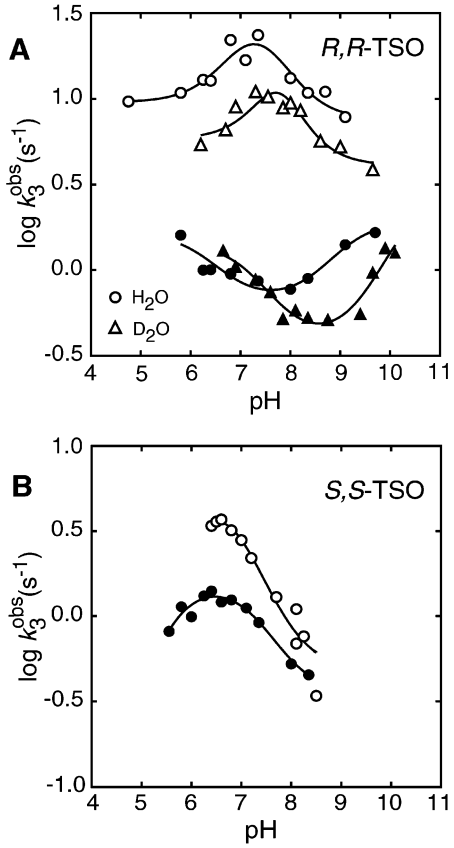

FIGURE 5: pH dependence of the hydrolysis of the alkylenzyme intermediate, k_3, catalyzed by the wild-type (○ and △) or E35Q mutant (● and ▲) enzymes, during hydrolysis of *R,R*-TSO (A) or *S,S*-TSO (B). Observed values of k_3 were determined under single-turnover conditions at different pH values (see Materials and Methods for details). The effect of pH/pD on k_3 for wild-type- or E35Q mutant-catalyzed reactions with *R,R*-TSO. The reaction performed in 100% H_2O (○ and ●) or 84.1% D_2O (△ and ▲) is given in panel A. Lines represent the fits of eq 5, describing titration of a doubly ionizing system, to the experimental data. Data for $k_3^{S,S-TSO}$ were adapted from ref *9*.

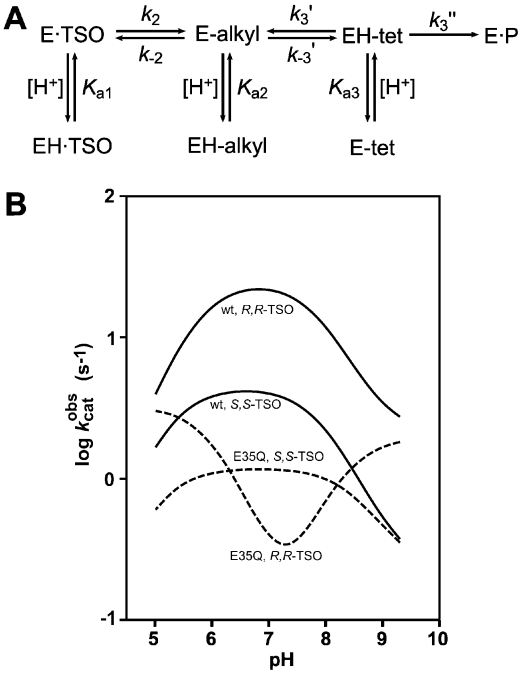

FIGURE 6: Computer simulation of the pH dependence of k_{cat} of TSO hydrolysis catalyzed by StEH1-5H and the E35Q mutant. (A) Proposed kinetic mechanism of k_{cat}-determining steps during TSO hydrolysis. The parameters k_2 and k_{-2} are the rates of the forward and reverse reactions for alkylenzyme (E-alkyl) formation and k_3' and k_3'' the rates of formation and breakdown of the tetrahedral intermediate (E-tet), respectively, and k_{-3}' is the rate of the reverse reaction from the tetrahedral intermediate to the alkylenzyme. The acid constants K_{a1}, K_{a2}, and K_{a3} describe the acidity of the enzyme−substrate complex and the alkylenzyme and tetrahedral intermediates, respectively. (B) Simulated curves of the pH dependence of k_{cat} obtained after entering the parameters given in Table 3 into eq 6. For details, see Materials and Methods.

resembling the experimentally determined ones (Figure 4) in the basic pH region, different intrinsic reactivities of the different alkylenzymes have to be invoked. This is not implausible considering their assumed alternative structures within the active sites.

The simulations of the kinetics, together with the experimental data collected at pH 6.8, suggest that the main effect on the reaction with *S,S*-TSO is a lowered alkylenzyme hydrolysis rate. With the *R,R* enantiomer, the mutation caused a decrease in both alkylation and hydrolysis rates. These effects, observed at pH 6.8, may be due to the change in acidity of His^{300} as suggested by the simulations of the kinetics.

Deuterium Solvent Isotope Effects

Since Glu^{35} participates in hydrogen bonding interactions both with the putative catalytic water and with residues connecting the active site with solvent through a hydrogen-bonded network, it was of interest to analyze any effects on rate-determining reactions involving proton transfer. Hence, possible deuterium solvent isotope effects on the main rate-limiting step, the alkylenzyme hydrolysis, were assayed for determination of k_3 in the presence of D_2O at different values of pH/pD. The results of the single-turnover experiments in the presence of *R,R*-TSO and wild-type or E35Q mutant StEH1-5H are depicted in Figure 5A and, with apparent kinetic pK_a values of $k_3^{D_2O}$, in Table 2.

For the wild-type-catalyzed reactions, the titration curves of k_3 in water or 84.1% deuterium oxide display similar shapes but with a clear kinetic solvent isotope effect over

Table 3: Applied Estimates of Kinetic Parameters and Relevant Acid Constants for Simulations of the pH Dependence of k_{cat} Supplemented with Calculated Values of His[300] pK_a

enzyme/substrate	pK_{a1}	pK_{a2}	pK_{a3}	k_2 (s^{-1})	k_{-2} (s^{-1})	k_3' (s^{-1})	k_{-3}' (s^{-1})	k_3'' (s^{-1})	k_0 (s^{-1})	pK_a^{lg} [a]
wild type/*R,R*-TSO	6.3	5.5	6.3	600	20	40	300	1000	2	8.3
E35Q/*R,R*-TSO	4.3	3.2	3.4	80	20	5	300	1000	2	8.3
wild type/*S,S*-TSO	5.0	5.3	6.3	80	20	10	60	200	0.2	8.3
E35Q/*S,S*-TSO	6.3	5.0	6.3	80	5	2	60	200	0.2	8.3

Calculated Values of His[300] pK_a

		Michaelis complex		alkylenzyme		tetrahedral intermediate	
	free enzyme	*R,R*-TSO	*S,S*-TSO	*R,R*-TSO	*S,S*-TSO	*R,R*-TSO	*S,S*-TSO
wild type	10.3 ± 1.5	10.7 ± 1.6	nd[b]	8.0 ± 1.8	7.9 ± 1.8	10.3 ± 1.8	nd[b]
E35Q	8.2 ± 1.0	8.4 ± 1.5	nd[b]	4.9 ± 1.9	4.8 ± 2.1	7.4 ± 1.5	nd[b]

[a] pK_a^{lg} is the estimated pK_a of the leaving group alcohol of the hydrolysis product bound to the enzyme active site. [b]Not determined.

the full analyzed pH/pD range. The pH/pD optimum of k_3 is shifted toward a more basic pH by 0.5 pH unit, a shift in agreement with earlier studies on the effect of D_2O on the k_{cat} of hydrolysis of phenanthrene 9,10-oxide catalyzed by rat microsomal epoxide hydrolase (*38*) and the His general base-catalyzed deacylation of α-chymotrypsin (*39*). The kinetic deuterium solvent isotope effect for $k_3^{R,R-TSO}$ ($k_3^{H_2O}/k_3^{D_2O}$) is 2.2, a value typical for general base-assisted ester hydrolysis (*39, 40*).

In the case of the alkylenzyme hydrolysis catalyzed by the E35Q mutant, the fitted pH or pD dependence curves, although inverted, display overall shapes similar to those of the titrations of the wild-type enzyme, but with a steeper slope of the basic limb of the titration curve in D_2O, resulting in an only minor solvent isotope effect at high pH/pD values (Figure 5A). The acidic limb is shifted ca. 0.5 pH or pD unit toward a more basic position but is roughly parallel to the corresponding titration in water. This behavior resembles the pH/pD dependence of k_{cat} in pepsin-catalyzed hydrolysis of model peptides (*41*). Hence, at pH values between 5.5 and 7.5, $k_3^{R,R-TSO}$ is dependent on a catalytic acid in the E35Q mutant with an apparent pK_a of 7.0, shifted to 7.3 in 84.1% D_2O (Table 2). Further, as judged by the deuterium solvent isotope effect of 2.1, at the rate minimum, hydrolysis of the alkylenzyme between pH 7.5 and 9 indeed involves rate-limiting proton transfer reactions.

Computer Simulations

To aid in the interpretation of the experimental results, the proposed catalytic mechanism and protonation state of His[300] were investigated using MD simulations and continuum electrostatic pK_a calculations.

Substrate-Free Enzyme. For the substrate-free form of StEH1, the crystallographic hydrogen bond network was disrupted in the MD simulation carried out with a neutral His[300]. However, for a charged His[300], the catalytic water was well-conserved and coordinated by Phe[33] O and Glu[35] Oε1. In this case, His[300] moves slightly toward the negatively charged Asp[105], forming a hydrogen bond to one of the carboxylate oxygens (Figure 7A). The pK_a of His[300] was estimated to be 10.3 ± 1.5.

E35Q Mutant. The alternative orientations of Gln[35] in the E35Q mutant were examined by carrying out simulations for the two conformers of the amide that can be obtained by replacing one of the Glu[35] Oε carboxylate oxygens with an NH_2 group. Starting from these two different alternatives in the substrate-free enzyme, both simulations converged to the suggested conformation, where the amide oxygen forms hydrogen bonds to the Ser[39] OH and Gln[304] NH_2 groups and the Gln[35] NH_2 group hydrogen bonds to His[104] Nε and Phe[33] O. Introduction of the E35Q mutation into the substrate-free structure also seems to push the catalytic water out of the active site. The estimated pK_a value indicates that the E35Q mutation decreases the pK_a value by 2 units to 8.2 ± 1.0 in the substrate-free enzyme.

Michaelis Complex and Alkylenzyme and Tetrahedral Intermediates. The calculated pK_a values of His[300] in the respective enzyme−substrate complexes with *R,R*-TSO suggest that formation of the Michaelis complex does not affect the acidity of the imidazolium to any major degree in either of the enzyme forms (Table 3). Formation of the alkylenzyme intermediate, however, reduces the corresponding pK_a values 2.7 and 3.5 pH units in the wild-type and E35Q enzymes, respectively, as compared to the noncovalent enzyme−substrate complexes. In the subsequent tetrahedral intermediates, formed in the reaction with *R,R*-TSO, the basicity of His[300] is again restored to levels resembling those of the states preceding alkylenzyme formation. Notably, the calculated pK_a values of the His[300] imidazolium in the E35Q mutant are at all steps of the reaction 2−3 units lower than the corresponding values of the wild type (Table 3).

Structures extracted from the simulations of the alkylenzyme intermediate show that the (charged) His[300]−Asp[105] hydrogen bond observed for the substrate-free enzyme is disrupted and, instead, His[300] forms a strong hydrogen bond to the catalytic water molecule (Figure 7B). In the MD simulations of the uncharged His[300], the catalytic water reorients and is coordinated by His[300] Nε and Phe[33] O.

It should be noted that the calculated pK_a values assume a standard value of the protein dielectric constant of 8, which has not been optimized for absolute agreement with experimental data. While such optimization would perhaps be possible, our main objective here is simply to explore the trends in pK_a shifts associated with the studied reaction.

DISCUSSION

Present View of StEH1-5H-Catalyzed Hydrolysis of TSO

The catalytic groups provided by the active sites of epoxide hydrolases have been identified through extensive structural and functional studies. The generic active site of an epoxide

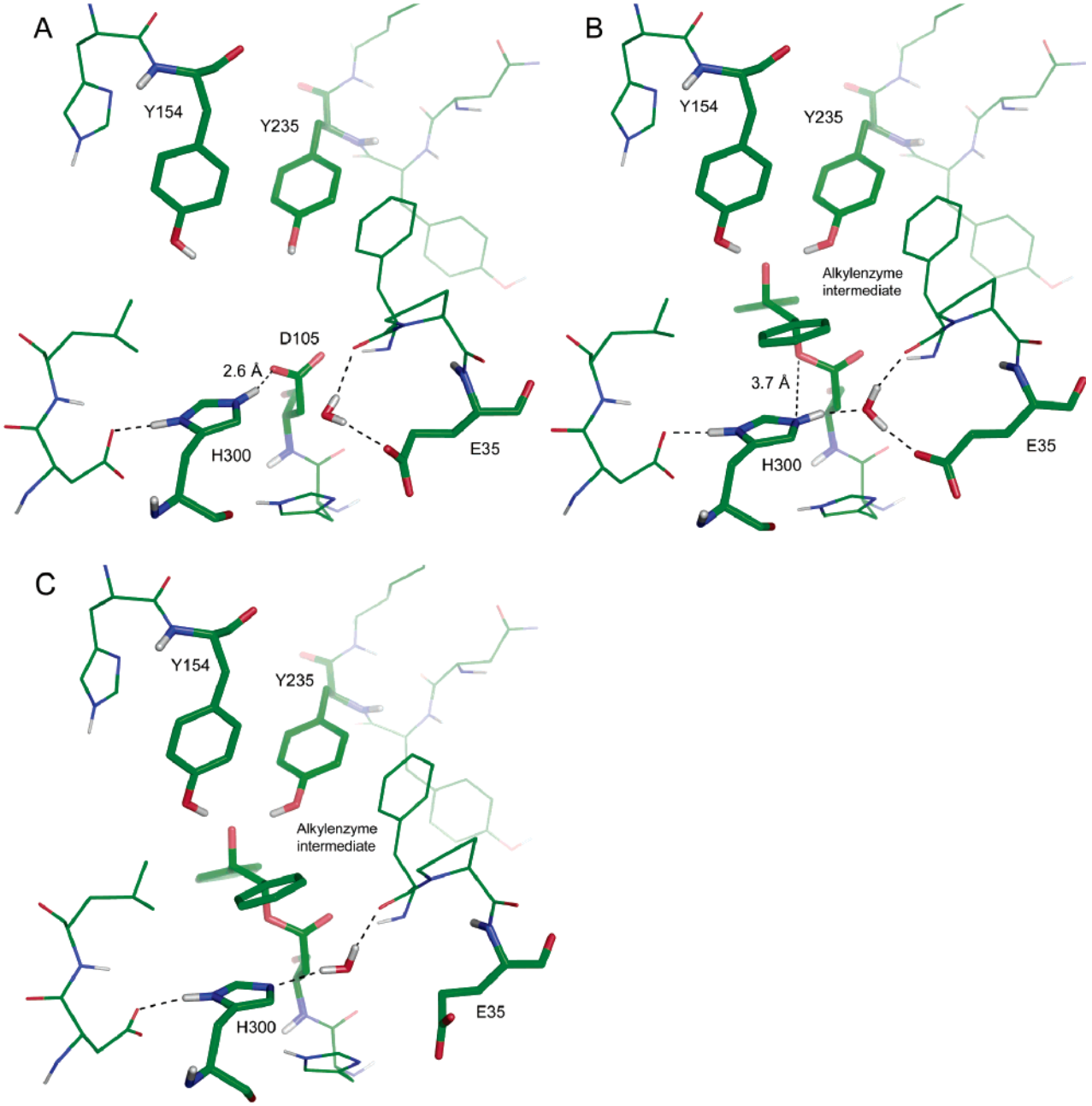

FIGURE 7: Average structures of the substrate-free and alkylenzyme intermediate forms extracted from 250 ps MD simulations. Selected hydrogen bond interactions are shown using black dashed lines. (A) Structure of the substrate-free enzyme with a charged His^{300}. His^{300} forms a hydrogen bond to Asp^{256} and Asp^{105} (the distance between the His^{300} Nϵ and Asp^{105} Oδ atoms is 2.6 Å), and the catalytic water is coordinated by Glu^{35} and Phe^{33}. (B) Alkylenzyme intermediate. Formation of the alkylenzyme intermediate from *R*,*R*-TSO leads to disruption of the hydrogen bond between Asp^{105} and (charged) His^{300} (the distance between the His^{300} Nϵ and Asp^{105} Oδ atoms is 3.7 Å), which reorients to act as a donor in a hydrogen bond to the catalytic water molecule. (C) In its deprotonated form, Nϵ of His^{300} acts as an acceptor in a hydrogen bond to the catalytic water molecule, allowing for general base activation for nucleophilic attack on the alkylenzyme. All images were created using PyMOL (*56*).

hydrolase of the α/β-hydrolase fold family provides a carboxylate nucleophile (*8*, *42*−*45*), attacking the epoxide ring to generate a covalent alkylenzyme (*45*−*48*). The reaction is facilitated by Tyr residues acting through electrophilic catalysis (*7*, *9*, *45*, *49*, *50*), and subsequently hydrolyzed in a general base-assisted reaction. The enzyme-provided His imidazole base (*8*, *42*, *45*, *48*, *51*) activates a water for nucleophilic attack of the alkylenzyme, forming a transient tetrahedral intermediate. As in other enzyme-catalyzed acyl transfer reactions, the tetrahedral intermediate is stabilized by fixed amide groups contributed by the polypeptide backbone. Decomposition of the tetrahedral intermediate and expulsion of the diol leaving group have been studied by computational methods (*52*) and are thought to be catalyzed by the active site His in its protonated imidazolium form.

Additional Catalytic Residues in Plant and Mammalian Epoxide Hydrolases?

Although all invoked catalytic steps may be identified by the described functional groups present in all characterized isoenzymes, it was conspicuous to identify yet another candidate catalytic residue in the active site of plant epoxide hydrolase StEH1. Glu^{35} protrudes its side chain carboxylate

within hydrogen bonding distance of the putative catalytic water (Figure 1). The high degree of conservation of the chemical properties as well as the structural features of interacting residues (Figure 2) drew further attention to its possible role in catalysis.

The position of Glu[35] in the active site and interactions made with neighboring residues imply distinct possible roles for this residue. Glu[35] is the first link in a chain of residues connecting the buried active site His[300] with bulk solvent through hydrogen bonding. Glu[35] thereby provides the entry of a plausible escape route for protons liberated during catalysis into solvent water or buffer bases, to facilitate maintenance of the net electrostatic neutrality in the active site throughout the reaction. His[300] is expected to become protonated during activation of the hydrolytic water (Figure 8, **V**) and when the side chain carboxylic acid of Asp[105] is released after hydrolysis of the alkylenzyme, at which point the acidic proton may be readily transferred to this nearby imidazole base (Figure 8, **VII**). It is also possible that the Glu[35] carboxylate could contribute to catalysis by a general base mechanism by additional polarization of the hydrolytic water together with the bona fide His[300] imidazole base, or by orienting the catalytic water for optimal base-catalyzed hydrolysis of the alkylenzyme. The catalytic gain from such a role would be from a lowering of the reaction order and the entropic losses during formation of the tetrahedral intermediate in the hydrolytic half-reaction (*53*).

The mutagenesis rationale, replacing Glu[35] with Gln, was to remove the acid−base functionality of the side chain carboxyl while causing a minimal disturbance of structural interactions. Although this mutation is considered to be surgical, in that presumably only the studied functional group was removed, the possibility that the properties of the E35Q mutant are particular to this enzyme variant cannot be excluded.

Hydrolysis of R,R- and S,S-TSO Catalyzed by StEH1-5H and the E35Q Mutant

Substrate-Free Enzyme. The calculated pK_a value of the His[300] imidazolium strongly suggests that this residue is positively charged at neutral pH. This is incompatible with a role as a general base and would require deprotonation prior to activation of the catalytic water. Furthermore, a protonated His[300] is well positioned to participate in ion−ion interaction with the carboxylate of the nucleophile Asp[105], thereby forming a salt bridge. Such a favorable interaction is expected to increase the pK_a of the imidazolium and lower the pK_a of the carboxyl group and may be one reason for the obtained value. Interestingly, the MD simulations of the substrate-free enzyme indeed support such an interaction (Figure 7A).

ES Complex Formation, Epoxide Ring Opening, and Formation of an Alkylenzyme Intermediate. It is clear from the rates for the different TSO enantiomers, of the wild-type enzyme-catalyzed formation of the respective alkylenzyme intermediates, that nucleophilic addition to *S,S*-TSO is less favorable, as compared to that of the *R,R* enantiomer. The obvious difference between these enantiomers is their potentially different binding modes in their respective Michaelis complexes, as also suggested by modeling (*10*). Different ES complex and alkylenzyme structures will influence the efficiencies in both the nucleophilic addition reaction of the epoxide carbon and the Asp[105] carboxylate and the stabilization of the alkoxide leaving group.

The alkylation rates of the E35Q mutant, however, do not display any clear differences between the enantiomers. The alkylation rate with *R,R*-TSO is lowered approximately 15-fold, at pH 6.8 (Table 1), to a rate similar to that displayed by the wild-type enzyme with *S,S*-TSO, whereas $k_2^{S,S-TSO}$ is apparently unaffected. The similarities of E35Q enzyme alkylation rates cannot easily be explained by an altered binding of the *R,R*-TSO substrate in the mutant, since the mutation per se is unlikely to affect relevant interactions. Therefore, a mechanism that incorporates both the enantioselective rate differences displayed by the wild-type enzyme and the loss in selectivity in the E35Q-catalyzed alkylation has to be sought. One possibility is that the proposed ion pair of His[300] and Asp[105] formed in the substrate-free enzyme is disrupted by binding of *R,R*-TSO in the active site, facilitating subsequent channeling of the imidazolium proton via the catalytic water to Glu[35] and further down the chain of hydrogen bonds (Figure 8, **II** and **III**). Binding of *S,S*-TSO to the wild-type enzyme (or binding of either enantiomer in the E35Q mutant) destabilizes the same salt bridge to a lesser extent. A persisting salt bridge is expected to depolarize the carboxylate, rendering it less nucleophilic and, hence, lowering the rate of enzyme alkylation, as observed. In the E35Q mutant, the connecting chain of hydrogen bonds from the active site His[300] to solvent water is assumed to be disrupted (Figure 3). If deprotonation of His[300] is required to promote enzyme alkylation and is dependent on an intact network of interactions, that function is lost in the mutant. The detailed reasons for the enantiospecific differences in k_2, at pH 6.8, displayed by the wild-type enzyme, however, are at this point uncertain.

Hydrolytic Half-Reaction: Formation and Decomposition of the Tetrahedral Intermediate. The main rate-limiting step in TSO conversion is the hydrolysis of the alkylenzyme with rate k_3 (Scheme 1). Experimental determinations of k_3 are based on measurements on the recovery of quenched intrinsic Trp fluorescence (*8*), which has been linked to formation of the preceding ionized alkylenzyme (*9*, *50*). A proposed model for the catalyzed formation and hydrolysis of the alkylenzyme is shown in Figure 8 (**III**−**VII**). The hydrolytic half-reaction is described as divided into two substeps. The first is a nucleophilic attack by a general base-polarized water molecule onto the alkylenzyme carbonyl to generate the transient tetrahedral intermediate (Figure 8, **V** and **VI**). In the MD simulations of the deprotonated His[300], the hydrolytic water molecule is well-aligned both for donation of a proton to Nϵ of His[300] and for nucleophilic attack on the alkylenzyme (Figure 7C). The second substep is decomposition of the tetrahedral intermediate with expulsion of the leaving group diol (Figure 8, **VI** and **VII**). The proposed mechanism involves protonation of the leaving group alkoxide by the His[300] imidazolium which is well-positioned for an acid role as judged by the crystal structure. Also, the corresponding His in human soluble epoxide hydrolase has, on the basis of energy calculations, recently been proposed to have a role as an acid catalyst in the breakdown of the tetrahedral intermediate that arises during hydrolysis of methylstyrene oxide (*52*). It has further been concluded from mechanistic studies of general base-catalyzed hydrolysis of esters with relatively poor leaving groups, e.g., aliphatic alkoxides, that

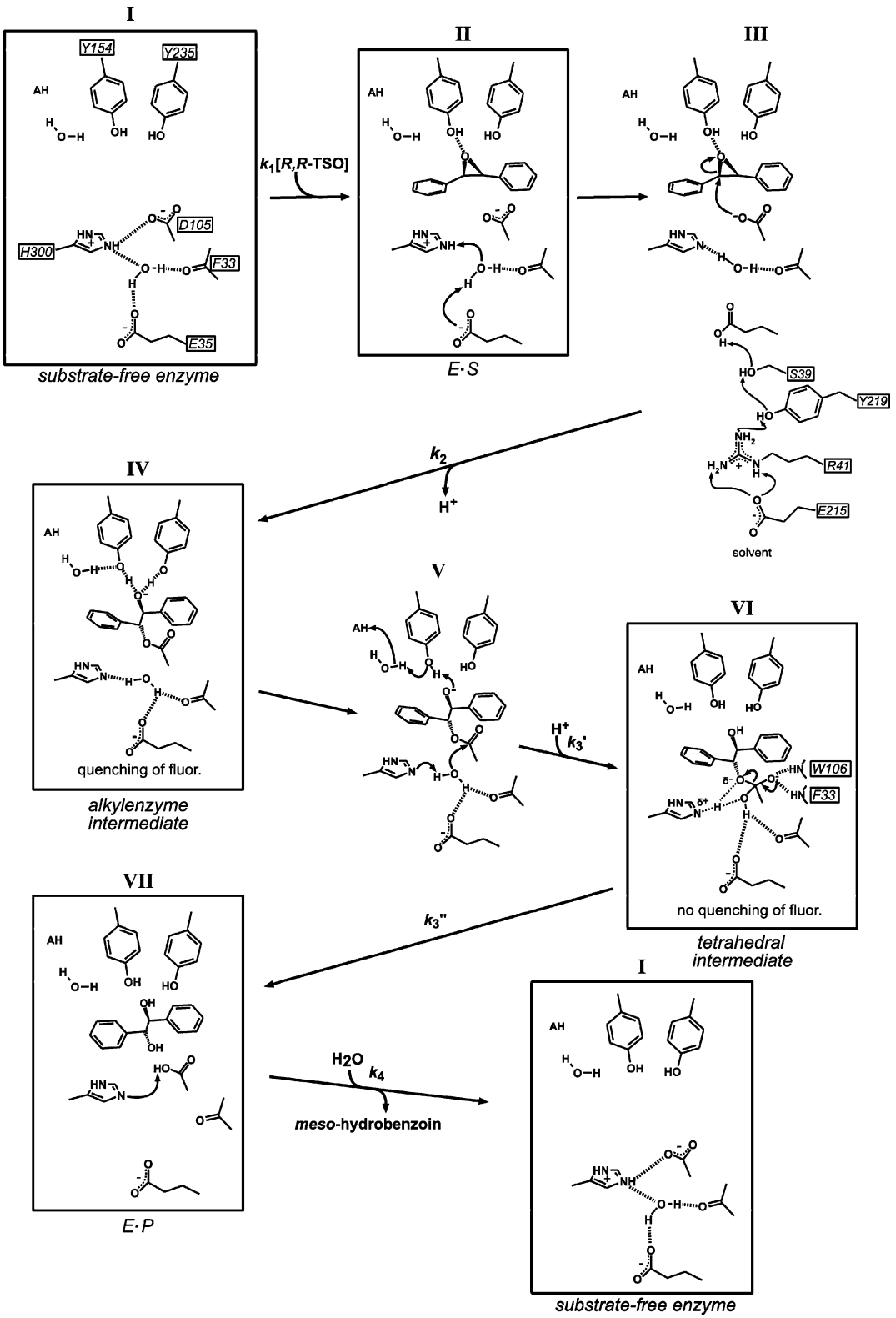

FIGURE 8: Proposed mechanism of StEH1-catalyzed TSO hydrolysis, based on spectroscopic, kinetic, and computer simulation data. (**I**) At neutral pH, the active site His^{300} is predominantly positively charged and participates in ion−ion interactions with Asp^{265} (not drawn) and Asp^{105}. The substrate enters into the active site and interacts with the protein primarily through nonpolar interactions and through a hydrogen bond between the epoxide oxygen and the Tyr^{154} hydroxyl (**II**). His^{300} is simultaneously deprotonated by a water-mediated base abstraction by Glu^{35}. The proton is further channeled to bulk solvent through a chain of hydrogen bond interactions involving side chains of Ser^{39}, Tyr^{219}, Arg^{41}, and Glu^{215} (**III**). Released from the ion pair interaction with His^{300}, Asp^{105} attacks the epoxide ring to form a charged alkylenzyme intermediate, stabilized by the phenols of Tyr^{154} and Tyr^{235} (**IV**). The alkylenzyme intermediate is subsequently attacked by a base-activated water to yield the tetrahedral intermediate (**V** and **VI**), stabilized by electrophilic catalysis provided by backbone amides of Phe^{33} and Trp^{106}. Concomitant with nucleophilic attack by this catalytic water, a proton is transferred from a chain of water molecules, via Tyr^{154}, to the charged alkylenzyme intermediate (**V**). Breakdown of the tetrahedral intermediate and expulsion of the leaving group diol product are facilitated by His^{300}-mediated acid catalysis (**VI** and **VII**). The enzyme is restored to the initial conformation after product release and binding of an additional catalytic water molecule. Dotted lines represent hydrogen bonds.

proton transfer to the leaving group contributes substantially to rate enhancement (*40*).

Restoration of the quenched Trp fluorescence signal is assumed to be an effect of protonation of the anionic alkylenzyme. If this process is coupled to formation of the tetrahedral intermediate or to its decomposition, product expulsion is unresolved. The expected unfavorable electrostatics resulting from an otherwise dianionic reaction intermediate, however, and the substantial differences in geometries and electrochemical properties of the tetrahedral intermediate and the alkylenzyme make it more likely that the formation of the tetrahedral intermediate triggers a concomitant protonation of the oxirane-originated alkoxide by water channeled into the active site [Figure 8, **V** (*9*)].

The pH dependence of k_{cat} of epoxide hydrolases, belonging to the α/β-hydrolase enzyme family, generally follows a bell-shaped pH dependence (*8*, *17*, *38*, *54*) with apparent pK_a values of 5−6.5 and 7.5−8.5 for the acidic and basic limbs of the titration curves, respectively. The acidic pK_a has been assigned to deprotonation of the active site His, required for general base catalysis of the rate-limiting alkylenzyme hydrolysis (Figure 8, **II**). Assignments of putative ionizable groups reflected by the titration of the basic limb, however, have remained elusive. The pH dependencies of k_3 are similar to that of k_{cat}, bell-shaped with apparent acid constants resembling those of k_{cat} in particular in the basic pH region (Figure 5 and Table 2). The calculated pK_a of approximately 10 for the imidazolium in the substrate-free enzyme is ≥4.5 pH units higher than the kinetic acidic pK_a for k_{cat} of TSO hydrolysis and 3.5 pH units above the pK_a of k_3 (Table 2). It follows that either the acidic limbs of the pH dependences of k_{cat} and k_3 do not solely reflect titrations of His^{300} or the pK_a of His^{300} varies over the duration of the catalytic cycle due to changes in microenvironment electrostatics between the different stages of the reaction. This would be analogous to the acid−base properties of the catalytic His in trypsin (*55*) and in accord with the calculated p$K_a^{His^{300}}$ which is lowered substantially going from the substrate-free to the respective alkylenzymes. Hence, the acidity of the His^{300} imidazolium during catalysis is reflected in the titrations of k_{cat} and k_3, rather than its acid−base characteristics in the substrate-free enzyme.

The two limbs of the pH dependence curves may also reflect different states of the same catalytic His residue, acting as a general base with an apparent pK_{a1} of approximately 6, catalyzing formation of the tetrahedral intermediate with a rate k_3', and with an apparent pK_{a2} of approximately 7.5, catalyzing the breakdown of the tetrahedral intermediate leading to diol expulsion. In the scheme of the kinetic mechanism for rate-limiting steps, i.e., reflected in k_{cat}, the measured rates of alkylenzyme hydrolysis are viewed as a composite of the rates of both the formation and breakdown of the tetrahedral intermediate (k_3' and k_3'' in Figures 6 and 8). Both of these steps depend on the acid−base properties of His^{300}, acting as a general base to promote formation of the intermediate and as an acid to catalyze its decomposition (Figure 8, **V** and **VI**). Therefore, observed values of k_{cat} can be expressed by the scheme in Figure 6A. The fluxes through the overall reaction are dependent on the kinetic rates and the protonation states of His^{300} at three different points: to promote formation of the alkylenzyme, to activate the catalytic water molecule for formation of the transient tetrahedral intermediate, and to facilitate leaving group expulsion. A change in the acidity of the His^{300} imidazolium, through the different reaction steps, would therefore affect the overall rate of catalysis. The simulations of the kinetic mechanism support this notion (Figure 6B and Table 3). In the k_{cat} simulations, which also mimic the inverted pH dependence of the E35Q−*R*,*R*-TSO pair, the imidazolium of the alkylenzyme is the most acidic species of all substrate−enzyme combinations. The results from the calculations of the pK_a of His^{300} also show that the acidity of this residue is highest in the alkylenzyme (Table 3). Furthermore, the relative differences in p$K_a^{His^{300}}$ are similar between the simulated and calculated pK_a values. Hence, the calculations support the proposal that it is the pK_a of His^{300} that changes over the catalytic cycle and that the removal of the negatively charged carboxylate in the E35Q mutant lowers its pK_a by approximately 2−3 pH units.

Role of Glu^{35}

It is clear from the collective data that the carboxylate of Glu^{35} is an integral part of the catalytic machinery of StEH1. The effects on catalytic function caused by the Gln replacement suggest that Glu^{35} participates both in activation of the Asp nucleophile by facilitating channeling of protons out of the active site and during the hydrolysis half-reaction. The role of Glu^{35} during alkylenzyme hydrolysis appears mainly to be to orient the catalytic water for optimal hydrogen bonding, thereby maintaining optimal acid−base characteristics of the His^{300} imidazolium, for facilitating both nucleophilic attack on the alkylenzyme and leaving group expulsion. It is worth noting that the functionality of Glu^{35} in the studied plant epoxide hydrolase is strongly conserved also in mammalian counterparts, implying that similar mechanisms prevail also in these important enzymes.

ACKNOWLEDGMENT

We thank Dr. Ylva Ivarsson and Diana Lindberg for constructive criticism during preparation of the manuscript.

REFERENCES

1. Arand, M., Cronin, A., Oesch, F., Mowbray, S. L., and Jones, T. A. (2003) The telltale of epoxide hydrolases, *Drug Metab. Rev. 35*, 365−383.
2. Morriseau, C., and Hammock, B. D. (2005) Epoxide hydrolases: Mechanisms, inhibitor designs and biological roles, *Annu. Rev. Pharmacol. Toxicol. 45*, 311−333.
3. Kolattukudy, P. E. (1981) Structure, biosynthesis, and biodegradation of cutin and suberin, *Annu. Rev. Plant Physiol. 32*, 539−567.
4. Fauth, M., Schweizer, O., Buchala, A., Markstädter, C., Riederer, M., Kato, T. and Kauss, H. (1998) Cutin monomers and surface wax constituents elicit H_2O_2 in conditioned cucumber hypocotyl segments and enhance the activity of other H_2O_2 elicitors, *Plant Physiol. 117*, 1373−1380.
5. Steinreiber, A., and Faber, K. (2001) Microbial epoxide hydrolases for preparative biotransformations, *Curr. Opin. Biotechnol. 12*, 552−558.
6. Archelas, A., and Furtoss, R. (2001) Synthetic applications of epoxide hydrolases, *Curr. Opin. Chem. Biol. 5*, 112−119.
7. Armstrong, R. N., and Cassidy, C. S. (2000) New structural and chemical insights into the catalytic mechanism of epoxide hydrolases, *Drug Metab. Rev. 32*, 327−338.
8. Elfström, L. T., and Widersten, M. (2005) Catalysis of potato epoxide hydrolase, StEH1, *Biochem. J. 390*, 633−640.

9. Elfström, L. T., and Widersten, M. (2006) Implications for an ionized alkyl-enzyme intermediate during StEH1-catalyzed trans-stilbene oxide hydrolysis, *Biochemistry 45*, 205−212.
10. Mowbray, S. L., Elfström, L. T., Ahlgren, K. M., Andersson, C. E., and Widersten, M. (2006) X-ray structure of potato epoxide hydrolase sheds light on substrate specificity in plant enzymes, *Protein Sci. 15*, 1628−1637.
11. Stapleton, A., Beetham, J. K., Pinot, F., Garbarino, J. E., Rockhold, D. R., Friedman, M., Hammock, B. D., and Belknap, W. R. (1994) Cloning and expression of soluble epoxide hydrolase from potato, *Plant J. 6*, 251−258.
12. Gomi, K., Yamamoto, H., and Akimitsu, K. (2003) Epoxide hydrolase: A mRNA induced by the fungal pathogen *Alternaria alternata* on rough lemon (*Citrus jambhiri* Lush), *Plant Mol. Biol. 53*, 189−199.
13. Katsube, T., Adachi, M., Maruyama, N., Ichise, K., Takenaka, Y., and Utsumi, S. (1995) Nucleotide sequence of a soybean cDNA encoding epoxide hydrolase, *Plant Physiol. 109*, 722−723.
14. Neuteboom, L. W., Kunimitsu, W. Y., and Christopher, D. A. (2002) Characterization and tissue-regulated expression of genes involved in pineapple (*Ananas comosus* L.) root development, *Plant Sci. 163*, 1021−1035.
15. Edqvist, J., and Farbos, I. (2003) A germination-specific epoxide hydrolase from *Euphorbia lagascae*, *Planta 216*, 403−412.
16. Kiyosue, T., Beetham, J. K., Pinot, F., Hammock, B. D., Yamaguchi-Shinozaki, K., and Shinozaki, K. (1994) Characterization of an *Arabidopsis* cDNA for a soluble epoxide hydrolase gene that is inducible by auxin and water stress, *Plant J. 6*, 259−269.
17. Bellevik, S., Zhang, J., and Meijer, J. (2002) *Brassica napus* soluble epoxide hydrolase (BNSEH1), cloning and characterization of the recombinant enzyme expressed in *Pichia pastoris*, *Eur. J. Biochem. 269*, 5295−5302.
18. Sasaki, T., Matsumoto, T., Yamamoto, K., Sakata, K., Baba, T., Katayose, Y., Wu, J., Niimura, Y., Cheng, Z., Nagamura, Y., Antonio, B. A., Kanamori, H., Hosokawa, S., Masukawa, M., Arikawa, K., Chiden, Y., Hayashi, M., Okamoto, M., Ando, T., Aoki, H., Arita, K., Hamada, M., Harada, C., Hijishita, S., Honda, M., Ichikawa, Y., Idonuma, A., Iijima, M., Ikeda, M., Ikeno, M., Ito, S., Ito, T., Ito, Y., Ito, Y., Iwabuchi, A., Kamiya, K., Karasawa, W., Katagiri, S., Kikuta, A., Kobayashi, N., Kono, I., Machita, K., Maehara, T., Mizuno, H., Mizubayashi, T., Mukai, Y., Nagasaki, H., Nakashima, M., Nakama, Y., Nakamichi, Y., Nakamura, M., Namiki, N., Negishi, M., Ohta, I., Ono, N., Saji, S., Sakai, K., Shibata, M., Shimokawa, T., Shomura, A., Song, J., Takazaki, Y., Terasawa, K., Tsuji, K., Waki, K., Yamagata, H., Yamane, H., Yoshiki, S., Yoshihara, R., Yukawa, K., Zhong, H., Iwama, H., Endo, T., Ito, H., Hahn, J. H., Kim, H.-I., Eun, M.-Y., Yano, M., Jiang, J., and Gojobori, T. (2002) The genome sequence and structure of rice chromosome 1, *Nature 420*, 312−316.
19. Guo, A., Durner, J., and Klessig, D. F. (1998) Characterization of a tobacco epoxide hydrolase gene induced during the resistance response to TMV, *Plant J. 15*, 647−656.
20. Newman, J. W., Stok, J. E., Vidal, J. D., Corbin, C. J., Huang, Q., Hammock, B. D., and Conley, A. J. (2004) Cytochrome p450-dependent lipid metabolism in preovulatory follicles, *Endocrinology 145*, 5097−5105.
21. Beetham, J. K., Tian, T., and Hammock, B. D. (1993) cDNA cloning and expression of a soluble epoxide hydrolase from human liver, *Arch. Biochem. Biophys. 305*, 197−201.
22. Knehr, M., Thomas, H., Arand, M., Gebel, T., Zeller, H.-D., and Oesch, F. (1993) Isolation and characterization of a cDNA encoding rat liver cytosolic epoxide hydrolase and its functional expression in *Escherichia coli*, *J. Biol. Chem. 268*, 17623−17627.
23. Grant, D. F., Storms, D. H., and Hammock, B. D. (1993) Molecular cloning and expression of murine liver soluble epoxide hydrolase, *J. Biol. Chem. 268*, 17628−17633.
24. Thompson, J. D., Higgins, D. G., and Gibson, T. J. (1994) CLUSTAL W: Improving the sensitivity of progressive multiple sequence alignment through sequence weighting, position specific gap penalties and weight matrix choice, *Nucleic Acids Res. 22*, 4673−4680.
25. Gomez, G. A., Morriseau, C., Hammock, B. D., and Christianson, D. W. (2004) Structure of human epoxide hydrolase reveals mechanistic inferences on bifunctional catalysis in epoxide and phosphate ester hydrolysis, *Biochemistry 43*, 4716−4723.
26. Wixtrom, R. N., and Hammock, B. D. (1988) Continuous spectrophotometric assays for cytosolic epoxide hydrolases, *Anal. Biochem. 174*, 291−299.
27. Waley, S. G. (1992) An easy method for deriving steady-state rate equations, *Biochem. J. 286*, 357−359.
28. Jones, G., Willett, P., and Glen, R. C. (1995) Molecular recognition of receptor-sites using a genetic algorithm with a description of desolvation, *J. Mol. Biol. 245*, 43−53.
29. Jones, G., Willett, P., Glen, R. C., Leach, A. R., and Taylor, R. (1997) Development and validation of a genetic algorithm for flexible docking, *J. Mol. Biol. 267*, 727−748.
30. Marelius, J., Kolmodin, K., Feierberg, I., and Åqvist, J. (1998) Q: A molecular dynamics program for free energy calculations and empirical valence bond simulations in biomolecular systems, *J. Mol. Graphics Modell. 16*, 213−225.
31. Jorgensen, W. L., Maxwell, D. S., and TiradoRives, J. (1996) Development and testing of the OPLS all-atom force field on conformational energetics and properties of organic liquids, *J. Am. Chem. Soc. 118*, 11225−11236.
32. Jorgensen, W. L., Chandrasekhar, J., Madura, J. D., Impey, R. W., and Klein, M. L. (1983) Comparison of simple potential functions for simulating liquid water, *J. Chem. Phys. 79*, 926−935.
33. King, G., and Warshel, A. (1989) A surface constrained all-atom solvent model for effective simulations of polar solutions, *J. Chem. Phys. 91*, 3647−3661.
34. Lee, F. S., and Warshel, A. (1992) A local reaction field method for fast evaluation of long-range electrostatic interactions in molecular simulations, *J. Chem. Phys. 97*, 3100−3107.
35. Georgescu, R. E., Alexov, E. G., and Gunner, M. R. (2002) Combining conformational flexibility and continuum electrostatics for calculating pK_as in proteins, *Biophys. J. 83*, 1731−1748.
36. Alexov, E. G., and Gunner, M. R. (1997) Incorporating protein conformational flexibility into the calculation of pH-dependent protein properties, *Biophys. J. 72*, 2075−2093.
37. Nicholls, A., and Honig, B. (1991) A rapid finite-difference algorithm, utilizing successive over-relaxation to solve the Poisson-Boltzmann equation, *J. Comput. Chem. 12*, 435−445.
38. Armstrong, R. N., Levin, W., and Jerina, D. M. (1980) Hepatic Microsomal Epoxide Hydrolase. Mechanistic studies of the hydration of k-region arene oxides, *J. Biol. Chem. 255*, 4698−4705.
39. Bender, M. L., Clement, G. E., Kézdy, F. J., and Heck, H. D'A. (1964) The correlation of the pH (pD) dependence and the stepwise mechanism of α-chymotrypsin-catalyzed reactions, *J. Am. Chem. Soc. 86*, 3680−3690.
40. Jencks, W. P., and Carriuolo, J. (1961) General base catalysis of ester hydrolysis, *J. Am. Chem. Soc. 83*, 1743−1750.
41. Clement, G. E., and Snyder, S. L. (1966) The kinetics of the pepsin-catalyzed hydrolysis of N-acetyl-L-phenylalanyl-L-tyrosine methyl ester, *J. Am. Chem. Soc. 88*, 5338−5339.
42. Pinot, F., Grant, D. F., Beetham, J. K., Parker, A. G., Borhan, B., Landt, S., Jones, A. d., and Hammock, B. D. (1995) Molecular and biochemical evidence for the involvement of the Asp-333-His-523 pair in the catalytic mechanism of soluble epoxide hydrolase, *J. Biol. Chem. 270*, 7968−7974.
43. Rink, R., Fennema, M., Smids, M., Dehmel, U., and Janssen, D. B. (1997) Primary structure and catalytic mechanism of the epoxide hydrolase from *Agrobacterium radiobacter* AD1, *J. Biol. Chem. 272*, 14650−14657.
44. Laughlin, L. T., Tzeng, H.-F., Lin, S., and Armstrong, R. N. (1998) Mechanism of microsomal epoxide hydrolase. Semifunctional site-specific mutants affecting the alkylation half-reaction, *Biochemistry 37*, 2897−2904.
45. Blée, E., Summerer, S., Flenet, M., Rogniaux, H., Van Dorsselaer, A., and Schuber, F. (2005) Soybean epoxide hydrolase. Identification of the catalytic residues and probing of the reaction mechanism with secondary kinetic isotope effects, *J. Biol. Chem. 280*, 6479−6487.
46. Lacourciere, G. M., and Armstrong, R. N. (1993) The catalytic mechanism of microsomal epoxide hydrolase involves an ester intermediate, *J. Am. Chem. Soc. 115*, 10466−10467.
47. Hammock, B. D., Pinot, F., Beetham, J. K., Grant, D. F., Arand, M., and Oesch, F. (1994) Isolation of a putative hydroxyacyl enzyme intermediate of an epoxide hydrolase, *Biochem. Biophys. Res. Commun. 198*, 850−856.
48. Muller, F., Arand M., Frank, H., Seidel, A., Hinz, W., Winkler, L., Hanel, K., Blée, E., Beetham, J. K., Hammock, B. D., and Oesch, F. (1997) Visualization of a covalent intermediate between microsomal epoxide hydrolase, but not cholesterol epoxide

hydrolase, and their substrates, *Eur. J. Biochem. 245*, 490−496.
49. Yamada, T., Morisseau, C., Maxwell, J. E., Argiriadi, M. A., Christianson, D. W., and Hammock, B. D. (2000) Biochemical evidence for the involvement of tyrosine in epoxide activation during the catalytic cycle of epoxide hydrolase, *J. Biol. Chem. 275*, 23082−23088.
50. Rink, R., Kingma, J., Lutje Spelberg, J. H., and Janssen, D. B. (2000) Tyrosine residues serve as proton donor in the catalytic mechanism of epoxide hydrolase from *Agrobacterium radiobacter*, *Biochemistry 39*, 5600−5613.
51. Tzeng, H. F., Laughlin, L. T., and Armstrong, R. N. (1998) Semifunctional site-specific mutants affecting the hydrolytic half-reaction of microsomal epoxide hydrolase, *Biochemistry 37*, 2905−2911.
52. Hopmann, K. H., and Himo, F. (2006) Theoretical study of the full reaction mechanism of human soluble epoxide hydrolase, *Chemistry 12*, 6898−6909.
53. Bruice, T. C., and Benkovic, S. J. (1964) The compensation in $\Delta H^{\ddagger}$ and $\Delta S^{\ddagger}$ accompanying the conversion of lower order nucleophilic displacement reactions to higher order catalytic processes. The temperature dependence of the hydrazinolysis and imidazole-catalyzed hydrolysis of substituted phenyl acetates, *J. Am. Chem. Soc. 86*, 418−426.
54. Blée, E., and Schuber, F. (1992) Occurrence of fatty acid epoxide hydrolases in soybean (*Glycine max*). Purification and characterization of the soluble form, *Biochem. J. 282*, 711−714.
55. Kossiakoff, A. A., and Spencer, S. A (1981) Direct determination of the protonation states of aspartic acid-102 and histidine-57 in the tetrahedral intermediate of the serine proteases: Neutron structure of trypsin, *Biochemistry 20*, 6462−6474.
56. DeLano, W. L. (2002) *The PyMOL Molecular Graphics System*, DeLano Scientific, San Carlos, CA.

BI062052S